

Supplemental Information for: Gas-phase oxidation and nanoparticle formation in multi-element laser ablation plumes

Elizabeth J. Kautz¹, Alla Zelenyuk¹, Bharat Gwalani^{1,2}, Mark C. Philips³, and Sivanandan S. Harilal^{1,4}

¹Pacific Northwest National Laboratory, Richland, WA 99352, USA

²Present Address: Department of Materials Science and Engineering, North Carolina State University, Raleigh, NC 27606, USA

³James C. Wyant College of Optical Sciences, University of Arizona, Tucson, Arizona 85721, USA

⁴Department of Chemistry, Washington State University, Pullman, WA 99164, USA

Appendix S1: Target Material Fabrication and Characterization

The target used in the present study (a refractory high entropy alloy, RHEA) was fabricated via arc melting in an inert atmosphere, using high purity (99.9 %) elements. The remelting was performed 6 times to ensure homogeneous melting and distribution of alloying elements. The alloy was subsequently homogenized by annealing at 1200 °C for 24 hours under continuously flowing Ar, followed by furnace cooling. A section of the processed alloy was mounted and prepared using standard metallography techniques for electron microscopy characterization before laser ablation (LA)/laser produced plasma (LPP) generation.

The target microstructure before LA in addition to nanoparticle (NP) morphology, crystallography, and composition were characterized ex-situ via electron microscopy. The target microstructure was analyzed via scanning and transmission electron microscopy (SEM and TEM, respectively).

Appendix S2: Characterization of the laser generated nanoparticles and agglomerates

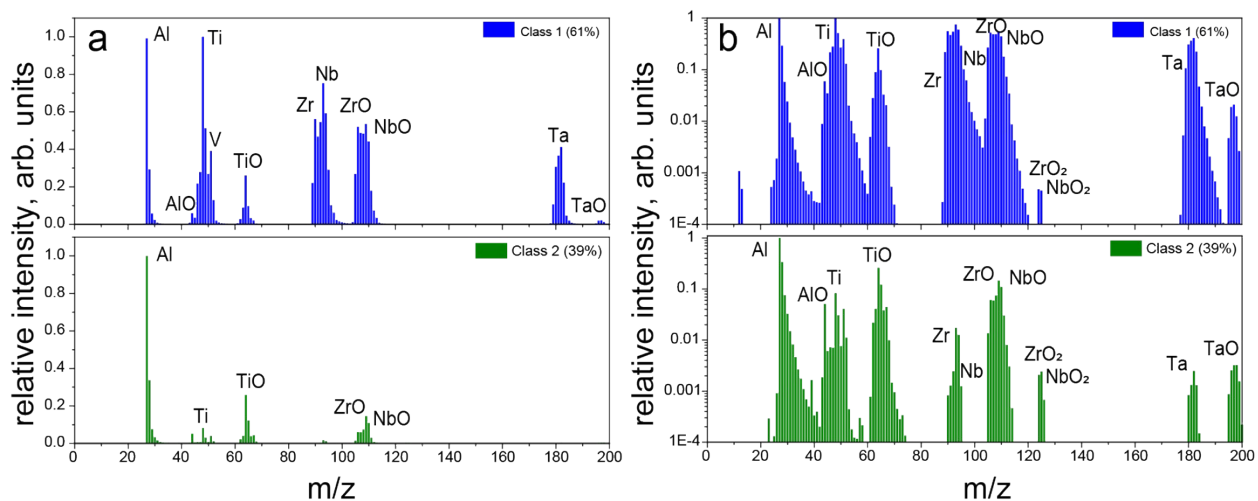


Figure S1: Average mass spectra of Class 1 and Class 2 plotted on linear (a) and logarithmic (b) scales for relative mass spectral intensities. Figure S2(b) makes it easier to see the presence of peaks with lower relative intensities. The comparison of Class 1 and Class 2 indicates that particles classified into Class 2 contain relatively larger fraction of oxidized species.

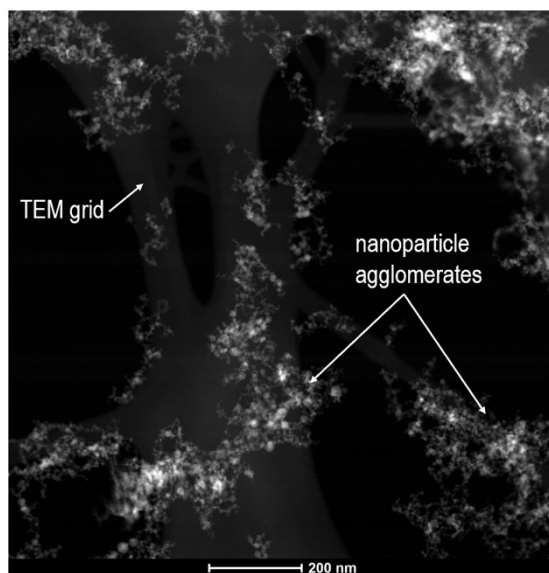


Figure S2: A high angle annular dark field (HAADF) STEM image shows a low magnification view of the nanoparticle fractals collected on a lacey Cu grid.

Appendix S3: Characterization of the target material before plasma generation

Prior to LA, the microstructure of the target material was imaged using SEM and TEM, with results reported in Figure S3. The SEM micrograph (Figure S3(a)) illustrates that the microstructure appears to be a single phase with grain size $\approx 165 \mu\text{m} \pm 72 \mu\text{m}$. A TEM foil was made from the center of a grain for a higher resolution examination of the alloy. The selected area diffraction pattern (SADP) given in Figure S3(b) is collected after aligning the body-centered cubic (BCC) structure of the alloy along the $\langle 001 \rangle$ direction which shows the presence of an ordered structure. The superlattice spot on the 010 positions correspond to the ordered BCC structure (i.e., B2). One such superlattice spot is selected to generate a darkfield TEM image (Figure S3(c)) highlighting the distribution of the B2 phase. The ordered B2 phase forms a continuous network (i.e., matrix) while the disordered BCC phase is distributed in the form of the cubes/cuboids within the B2 matrix. A Z-contrast-based image collected using the

HAADF detector in TEM (Figure S3(d)) shows the BCC phase appears brighter than the B2 phase and thus has a heavier average mass. The EDS maps showed that the B2 phase is rich in Al and Zr while the BCC phase contained higher Ta, Nb, Ti, and V. The Zr and Ta maps are provided in Figures S3(e) and (f), respectively, while further microstructural details regarding the composition and 3D distribution of the phases are detailed elsewhere.¹ Given this alloy system containing Ta and Zr which have a miscibility gap (up to $\approx 1800 \text{ K}$), the alloy could have undergone a phase separation during processing.¹ In the current work, LPPs were generated from this alloy using a relatively large spot size of $\approx 1 \text{ mm}$ that captures a large region (i.e., several grains) of this multi-phase target material. A combination of spectroscopy, spectrometry, and microscopy methods were used to track the transformation from this multi-phase, chemical heterogeneous target to particulate material formed in the LA process in a reactive, oxygen-containing environment.

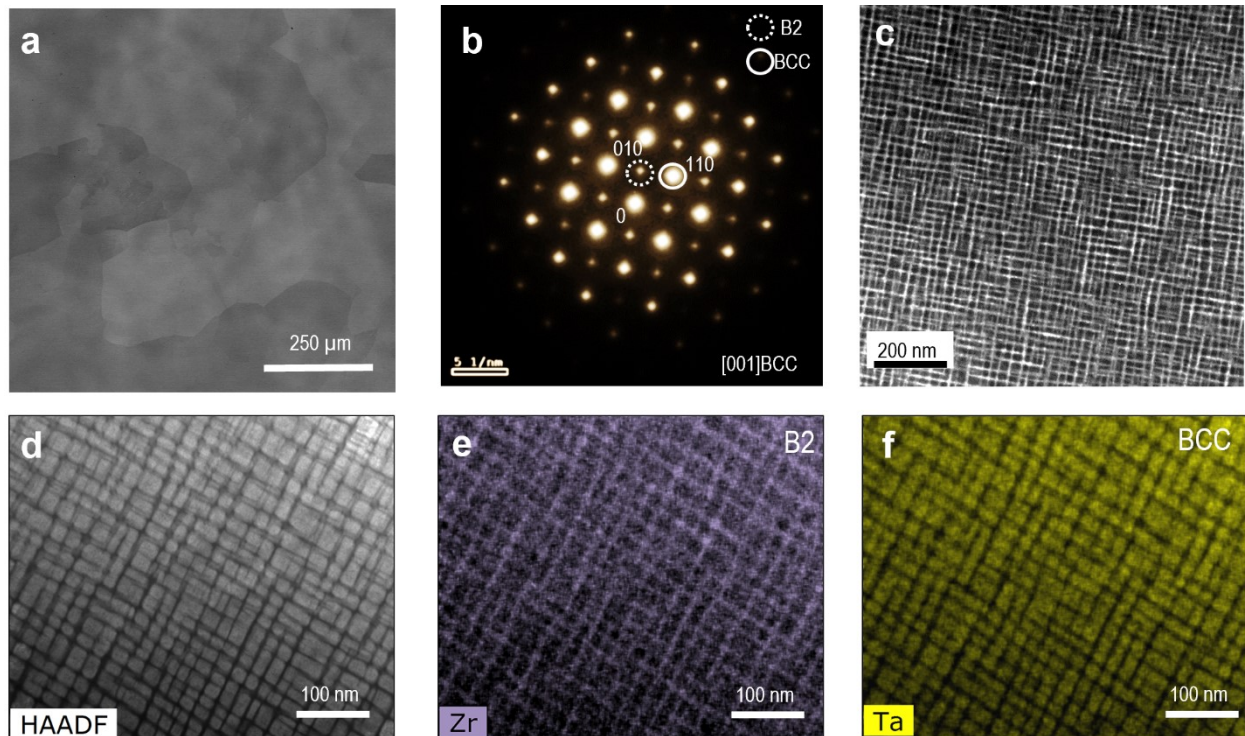


Figure S3: Electron microscopic imaging of the starting material prior to LA: (a) backscatter image from SEM; (b) selected area diffraction pattern (SADP) recorded after aligning the TEM foil along the $\langle 001 \rangle$ direction of the crystal; (c) dark field TEM image generated by selecting the superlattice spot corresponding to ordered B2 structure in the SADP shown in (b); (d) image showing the Z-contrast changes in the microstructure collect using high angle annular dark field detector in TEM; (e) EDS based compositional map showing the distribution of Zr in the microstructure. (f) EDS map showing the distribution of Ta. We noted that the Al and Zr prefer to partition towards the ordered B2 phase while the Ta, Nb, and Ti preferred to partition toward the BCC phase.

References

1. V. Soni, B. Gwalani, T. Alam, S. Dasari, Y. Zheng, O.N. Senkov, D. Miracle, R. Banerjee, *Acta Materialia*, 2020, **185**, 89-97.